ENVIRONMENTAL RESEARCH
COMMUNICATIONS

INCLUSIVE PUBLISHING
TRUSTED SCIENCE

Part of the
ENVIRONMENTAL RESEARCH
SERIES

PURPOSE-LED
PUBLISHING™

PAPER • **OPEN ACCESS**

Salinity-driven dynamics in the central Mediterranean in the era of ocean warming

To cite this article: Milena Menna *et al* 2026 *Environ. Res. Commun.* **8** 045002

Environmental Research Communications

OPEN ACCESS

RECEIVED
19 January 2026

REVISED
13 March 2026

ACCEPTED FOR PUBLICATION
20 March 2026

PUBLISHED
1 April 2026

PAPER

Salinity-driven dynamics in the central Mediterranean in the era of ocean warming

Milena Menna*, Miroslav Gačić, Annunziata Pirro, Elena Mauri, Gilda Savonitto, Massimo Pacciaroni, Vanessa Cardin, Giulio Notarstefano, Antonella Gallo, Piero Zuppelli, Antonio Bussani and Riccardo Martellucci

Oceanography section, National Institute of Oceanography and Applied Geophysics, Borgo Grotta Gigante 42/c 34010 Sgonico (TS), Italy
* Author to whom any correspondence should be addressed.

E-mail: mmenna@ogs.it

Keywords: central Mediterranean, salinity gradients, vorticity, current field IOP

Abstract

Scientists are closely monitoring the effects of global warming on the oceanic conveyor belt because of its central role in maintaining global climate stability. As the oceans warm up and become more stratified, processes driven by salinity are becoming increasingly important in shaping surface circulation, despite traditionally being considered less significant than wind forcing and sea-level gradients. This study examines salinity-driven dynamics in the Central Mediterranean Sea (CMed) using an integrated approach combining *in situ* observations (Argo floats and gliders), satellite data and model reanalysis. The CMed is a critical region where the zonal and meridional branches of the Mediterranean overturning circulation converge and deep convection and dense water formation occur. Over recent decades, the region has experienced significant warming and salinification, with salinity levels rising sharply since 2012. This enhanced salinity has directly affected the circulation field and the vertical stability of the water column. In the Southern Adriatic Gyre, the vorticity field is primarily driven by wind forcing and its interannual variability, but is also strongly influenced by horizontal advection from adjacent regions. After 2012, the baroclinic term of the vorticity equation associated with salinity-induced density gradients became increasingly significant, reaching magnitudes comparable to wind stress. Together with advection, these effects shaped the circulation. In the North Ionian Sea, rising upper-layer salinity has intensified the centre–edge salinity gradient during the inflow of fresher, Atlantic-origin waters. This has led to a weakening of the vorticity field and increased water-column stability. These findings highlight the growing importance of salinity in driving thermohaline variability and surface circulation, with significant implications for the dynamics of the Mediterranean Sea in the context of ongoing climate change.

1. Introduction

The impact of global warming on the oceanic conveyor belt is currently being extensively studied and monitored because of its known effects on global climate (O'Hare 2011, Hu *et al* 2013). In this context, the Mediterranean Sea, which is considered a hotspot for climate change and is characterized by a relatively short residence time of water masses (~150 years; Schneider *et al* 2010, 2014, Schroeder *et al* 2020) compared to the global ocean (~1000 years; England 1995), is a useful region for studying changes in thermohaline circulation.

Within the Mediterranean, the Central Mediterranean (CMed), consisting of the Ionian and Adriatic seas (figure 1(a)), can be considered a good indicator of variability for many reasons. First, it is a crossroads for all waters involved in the zonal Mediterranean overturning circulation (Menna *et al* 2019, Pinardi *et al* 2019, Kassis and Korres 2021, Civitarese *et al* 2023, Eusebi Borzelli *et al* 2025, Terzić *et al* 2025), that is the Atlantic Water (AW) and the Levantine Intermediate Water (LIW). Second, including one of the sites of open-ocean deep convection as well as regions of dense and deep-water formation of the Mediterranean Sea, the CMed can be

considered a connecting area between the zonal and meridional overturning cells. Moreover, it is considered a gauge of quasi-decadal variability of the whole Mediterranean (Gačić *et al* 2013, Menna *et al* 2022a, Placenti *et al* 2022, Meli 2024).

The CMed is a complex dynamic system, closely linked to the interaction between internal and external forcings that vary on interannual and quasi-decadal timescales (Menna *et al* 2019, 2022a). Its basin-scale circulation is strongly influenced by quasi-decadal reversals of the North Ionian Gyre (NIG) at the surface and by the production and storage of Adriatic Dense Water (AdDW) and Eastern Mediterranean Deep Water (EMDW) in its deeper layers (Manca *et al* 2002, Bensi *et al* 2016). The Adriatic Sea is the northernmost sub-basin of the CMed and is influenced by prominent winter heat losses, making it a dense water formation site (Mantziafou and Lascaratos 2004, Verri *et al* 2018, Shabrang *et al* 2016, Pirro *et al* 2022, Paladini de Mendoza *et al* 2023). Specifically, strong northeasterly winds (Bora) bring cold and dry continental air over the sea, causing latent and sensible heat losses (Manca *et al* 2003), which leads to the production of North Adriatic dense water (NAddW; Vilibić *et al* 2023, Schroeder *et al* 2024). The deepest part of the Adriatic Sea is the South Adriatic Pit (SAP), characterized by cyclonic circulation (the Southern Adriatic Gyre—SAG; inset of figure 1(a)) trapped by the topography and forced by prevailing winds. This cyclonic gyre consists of a northward eastern branch (Eastern Adriatic Current - EAC) that enters the Adriatic through the Otranto Channel (Poulain and Cushman-Roisin 2001, Gačić *et al* 2002, Lipizer *et al* 2014), and an outflowing, low-saline western branch (Western Adriatic Current—WAC), influenced by river discharges in the northern area of the basin (Lipizer *et al* 2014). The SAG is the site of AdDW formation, representing the main component of the EMDW, which occupies the bottom layer of the entire eastern Mediterranean (Manca *et al* 2002). Vertical convection processes in this region and their related structures and drivers have been studied in recent years (Cardin *et al* 2020, Pirro *et al* 2022, Paladini de Mendoza *et al* 2023, Di Biagio *et al* 2023, Amorim *et al* 2024, Martellucci *et al* 2024, 2025, Le Meur *et al* 2025). The complex thermohaline circulation of the South Adriatic is driven by the interaction between different processes: wintertime dense water formation events (Gačić *et al* 2002), the inflow of fresher water from the northern Adriatic rivers (Vilibić *et al* 2013, Pranić *et al* 2023), the dense water produced in the North Adriatic (Bensi *et al* 2013), and the inflow/outflow of surface-intermediate/dense water masses from/to the Otranto Channel (Yari *et al* 2012, Menna *et al* 2022a, 2022b).

The Ionian Sea is divided into two sub-basins by a zonal, intense, meandering current known as the Mid-Ionian Jet (MIJ; figure 1(a)). The circulation in the southern Ionian is characterized by a permanent anticyclonic structure located off the Libyan coast and is defined as the Syrte Gyre (Menna and Poulain 2010, Poulain *et al* 2012, Pinardi *et al* 2015, Menna *et al* 2022a). In contrast, the current field of the North Ionian is dominated by the periodic reversal of the NIG (figures 1(b) and (c)), anticyclonic to cyclonic modes, and vice-versa (Gačić *et al* 2010, Menna *et al* 2019, Gačić *et al* 2021, Menna *et al* 2022a, 2022b, Civitarese *et al* 2023). NIG reversals affect the water mass distribution among the Eastern Mediterranean sub-basins (Gačić *et al* 2011, Bessières *et al* 2013, Reale *et al* 2017, Notarstefano *et al* 2019, Kassis and Korres 2021, Ozer *et al* 2022, Pirro *et al* 2024), in turn influencing the sea level (Menna *et al* 2022a, Meli 2024) and the thermohaline properties (Gačić *et al* 2013, Schroeder *et al* 2017, Menna *et al* 2022a, Pirro *et al* 2024) of the whole Mediterranean on decadal and multi-decadal scales. During the anticyclonic phase of the NIG, the AW is deflected northeastward toward the North Ionian and Adriatic Sea (figure 1(b)), resulting in the weakening of the MIJ. This condition leads to a reduced inflow of AW in the Levantine basin, resulting in saltier Levantine Surface Water (LSW; Gačić *et al* 2014) and a density decrease in the Adriatic, which produces and exports a less dense AdDW. The cyclonic phase of the NIG (figure 1(c)) allows the inflow of more saline water masses of Levantine origin into the Adriatic Basin and enhances the inflow of AW in the eastern Mediterranean (Menna *et al* 2021). This mechanism facilitates winter convection in the South Adriatic area and leads to the formation of a denser AdDW; simultaneously, the lowering of the sea level along the flanks of the Ionian results in the weakening of the upper-layer cyclonic circulation (Gačić *et al* 2010).

Surface currents play a key role in determining the thermohaline structures in the upper ocean, modulating both the mean state and the interannual variability. Conversely, the thermohaline structure and its variability can also affect surface currents by altering the ocean density and pressure gradients (Chen *et al* 2021). Currently, the effects of thermohaline properties on surface currents are not well studied or understood, particularly regarding the role of salinity, as it is considered less important than other factors affecting the circulation field, such as wind and sea level. However, in an era characterized by ocean warming, which impacts ocean stratification (Li *et al* 2020) and increases sea levels (von Schuckmann *et al* 2018, Menna *et al* 2022a, Meli *et al* 2023), the contribution of ocean density to the upper layer circulation becomes significant. In particular, salinity can play a leading role in shaping thermohaline variability by compensating for or enhancing temperature-driven density changes and controlling the processes that govern dense water formation.

In recent decades, significant positive trends in salinity and temperature have been observed in the water column of the CMed (Mihanović *et al* 2021 Menna *et al* 2022a, Kubin *et al* 2023, Amorim *et al* 2024, Martellucci *et al* 2024, Terzić *et al* 2025, Terzic & Vilibic 2026). These trends, along with more frequent reversals of the NIG

(Menna *et al* 2022b, Civitarese *et al* 2023, Eusebi Borzelli and Carniel 2023) and the interannual variability of the main dynamic structures in the area (Menna *et al* 2019), highlight significant changes in the region. In this context, the present study aims to define the role of thermohaline properties in shaping the variability of the surface current field of the CMed. This analysis was conducted using *in situ*, satellite, and model-derived products, focusing on two critical regions of the CMed: the SAG and the NIG.

2. Method

The datasets used in this study were obtained from satellite products (sea level and geostrophic currents derived from altimetry), *in situ* data (temperature and salinity derived from historical datasets, Argo floats, and ocean gliders), and model reanalysis (wind speed, temperature, and salinity) covering the period from 1993 to 2023. This section provides a brief description of the datasets and methods used for their analysis.

The daily (1/8° Mercator projection grid) Absolute Dynamic Topography (ADT) and corresponding Absolute Geostrophic Velocities (AGV) derived from altimeters and distributed by CMEMS (product user manual CMEMS-SL-QUID_008-032-051) were downloaded from the Copernicus Marine Services (https://doi.org/10.48670/moi-00148). The ADT was obtained by adding the sea-level anomaly to the 20-years synthetic mean estimated by Rio *et al* (2014) over the 1993–2012 period. The mean ADT maps for 1995 (figure 1(b)) and 2004 (figure 1(c)) were used to describe the anticyclonic and cyclonic conditions of the NIG, respectively. The monthly fields of the AGV were derived to estimate the relative vorticity and horizontal volume transport in the CMed. Relative vorticity (ζ), defined as the vertical component of the curl of the geostrophic velocity field, is expressed as follows:

$$\zeta = \frac{\partial v}{\partial x} - \frac{\partial u}{\partial y}; \tag{1}$$

where u and v are zonal and meridional velocity components, respectively. The resulting fields were used to derive the time series of the spatially averaged relative vorticity over the NIG (37–39°N; 17–19.5°E; red box in figure 1(a); Notarstefano *et al* 2019) and SAG (area delimited in red by the 1000 m bathymetry, figure 1(a)) subregions. Subsequently, we evaluated the relative importance of the different terms in the potential vorticity equation in SAG. As the relative vorticity was derived from the AGV data, which do not provide information on the current field within the water column and near the bottom, the contributions of tube stretching and bottom stress were neglected. The resulting vorticity equation is as follows:.

$$\frac{\partial \zeta}{\partial t} = -V\cdot\nabla\zeta + \frac{\nabla p \times \nabla \rho}{\rho_0^2} + \frac{1}{\rho_0 D}[curl\tau]_z; \tag{2}$$

where the first term ($-V\cdot\nabla\zeta$) is the advection from neighboring areas; the second term is the baroclinic term, with p and ρ_0 being the pressure and density (1025 kg·m^{-3}) of seawater, respectively; the third term describes the wind-driven contribution to the vorticity field, with D being the thickness of the upper layer (0-MLD m depth) and $[curl\tau]_z$ being the vertical component of the wind-stress curl:

$$[curl\tau]_z = \frac{\partial \tau_y}{\partial x} - \frac{\partial \tau_x}{\partial y}; (\tau_x, \tau_y) = \rho C_D (u_w, v_w) V_{10}; \tag{3}$$

where (τ_x, τ_y) are the wind-stress components; ρ (1.22 kg·m^{-3}) is the density of air; (u_w, v_w) and V_{10} are the components and magnitude of the wind speed at 10 m, respectively; and C_D is the drag coefficient used in the Mediterranean Sea by Shabrang *et al* (2016), Menna *et al* (2019), and Menna *et al* (2023). Wind velocity gridded data (with a spatial resolution of 31 km and temporal resolution of 12 h) were downloaded from the ECMWF ERA5 global atmospheric reanalysis (https://www.ecmwf.int/en/forecasts/dataset/ecmwf-reanalysis-v5). The order of magnitude of the baroclinic term was estimated following Gačić *et al* (2010) as $O\left(\frac{f^2V^2}{gD}\right)$, where g is the gravitational acceleration.

To describe the interannual variability of the horizontal advection, we used the meridional component of the horizontal volume transport as a proxy, estimated across two zonal transects located on the eastern and western edges of the SAG (figure 1), using the method described by Pinardi *et al* (2019).

Time series of *in situ* temperature and salinity were obtained from the data derived from the World Ocean Dataset and Argo float profiles (Argo 2020, Wong *et al* 2020, Sunanda *et al* 2025). Most float profiles used in this study were validated using the Delayed Mode Quality Control (DMQC) technique (Cabanes *et al* 2021). The strategy adopted for DMQC has been widely described in the literature (Wong *et al* 2003, Böhme and Send 2005, Owens and Wong 2009, Notarstefano and Poulain 2013, Cabanes *et al* 2016, 2021). The accuracy of the salinity measurements requested by Argo after the DMQC was 0.01. When DMQC data were unavailable, real-time data were used. Argo float and WOD monthly salinity profiles were vertically averaged in the upper (100–200 m) and intermediate (200–800 m) layers and were then grouped into two different sub-regions in the

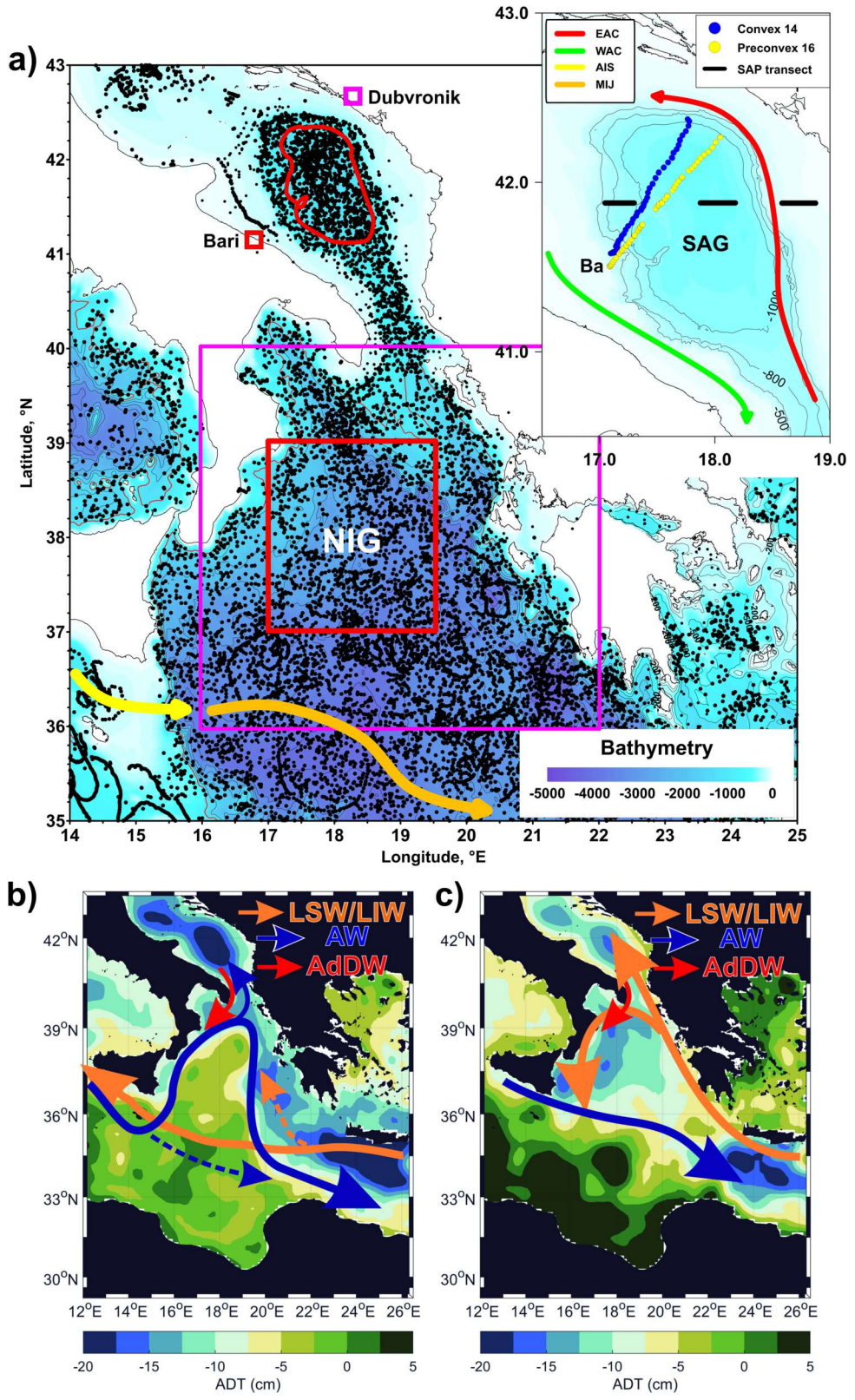

Figure 1. Geographical location of Argo float profiles (a) in the CMed (black dots) superimposed on the bathymetry of the area. The subregions circled in red and magenta define the areas used to estimate the time series of vorticity, temperature and salinity. Glider sections (blue and yellow dots) and the location of the transects used to define the centre, western and eastern edges of the Southern Adriatic Gyre (black transects) are shown in the inset. Schematic representation of the water mass distribution (orange and blue arrows) during the NIG (b) anticyclonic (c) cyclonic modes superimposed on the mean ADT field in (b) 1995 and (c) 2004. Acronyms: SAG—South Adriatic Gyre; NIG—Northern Ionian Gyre; AW—Atlantic Water; LSW—Levantine Surface Water; LIW—Levantine Intermediate Water; AdDW—Adriatic Deep Water; AIS - Atlantic-Ionian Stream; MIJ - Mid-Ionian Jet; EAC - Eastern Adriatic Current; WAC - Western Adriatic Current; WCS—Western Cretan Straits; CP—Cretan Passage.

NIG and SAG areas. Monthly salinity and temperature averages were obtained for each subregion and layer. Linear salinity trends were estimated separately in the intermediate layer for the periods characterized by cyclonic and anticyclonic NIG.

Evaporation (E), precipitation (P), and runoff (Rf) data were downloaded from the monthly ERA5 reanalysis at a spatial resolution of 0.25° Lat. x 0.25° Lon. (Hersbach *et al* 2020). The time series of the freshwater flux, defined as E-(P + RF), was obtained for the SAG sub-region by spatially averaging the monthly fields over the area coordinates.

The glider data collected during the Convex 2014 (16–22 February 2014) and PreConvex 2016 (20–26 November 2015) field campaigns were part of a long project started in 2013, focusing on monitoring the dense water formation in the SAP during the preconditioning (November–December) period and the mixing/spreading (January–March) phase (Pirro *et al* 2022). To this end, the Bari (Ba)–Dubrovnik (Du) transect was conducted twice a year during winter. Glider data from Convex 2014 were corrected using moored E2M3A buoy and float data. Both glider data collected during Convex 2014 and PreConvex 2016 were subjected to quality control procedures in the delayed mode (https://doi.org/10.6092/ea0d979a-4043-4cf1-9397-6e097c315591).

The monthly surface temperature and salinity fields (0–150 m depth) were derived from the Copernicus Marine Service Analysis and Forecast physical product (https://doi.org/10.25423/CMCC/MEDSEA_MULTIYEAR_PHY_006_004_E3R1) distributed by CMEMS (hereafter MEDSEA). This product was assessed using a variational data assimilation scheme for temperature and salinity vertical profiles, SST, and satellite sea level anomalies along track data (Escudier *et al* 2020). These products were used to define the center-to-edge gradients of temperature and salinity in the SAG and the stratification of the water column. Temperature and salinity differences were estimated along a transect at 41.9°N. The center (C) of this transect was defined by the 17.6–18.1°E segment, whereas the western (Ew) and eastern (Ee) edges were defined by the 16.8–17.3°E and 18.5–19°E segments, respectively. The differences in temperature and salinity between C and the Ew and Ee edges in the layer 0–150 m were defined as (ΔTC-ΔTEw; ΔSC-ΔSEw) and (ΔTC-ΔTEe; ΔSC-ΔSEe), respectively.

Stratification N^2 was computed using the equation of state (TEOS-10; IOC, SCOR and IAPSO 2010). To evaluate the relative contributions of temperature and salinity to the change in N^2 in the upper 150 m, we followed Li *et al* (2020).

Linear trends were estimated for *in situ* temperature and salinity. Trends' significance was evaluated using the Mann–Kendall test, a nonparametric method commonly employed to detect monotonic trends in a series of environmental, climate, or hydrological data. The trends estimated in this work passed the test (the null hypothesis was rejected; 95% confidence level).

Monthly time series of vorticity, the meridional component of the volume transport, *in situ* temperature, N^2 and freshwater flux were filtered using a 13-month moving average to remove seasonal variations and focus on interannual fluctuations.

3. Results

The time series of vertically averaged salinity in the upper (100–200 m) and intermediate (200–800 m) layers showed a positive linear trend from the 1990s in both the South Adriatic (figure 2(a); upper layer 0.007 psu·year^{-1}; intermediate layer 0.008 psu·year^{-1}) and North Ionian sub-basins (figure 2(b); upper layer 0.013 psu·year^{-1}; intermediate layer 0.006 psu·year^{-1}). A steep increase in salinity began in 2012 (figures 2(a), (b); black lines; South Adriatic upper layer 0.024 psu·year^{-1}; intermediate layer 0.022 psu·year^{-1}; North Ionian upper layer 0.014 psu·year^{-1}; intermediate layer 0.016 psu·year^{-1}), with record-breaking values observed in 2021 (maximum salinity of 39.35 on October 2, at a depth of 9 m). This increase in salinity from 2012 is hereafter defined as the salinification process of the CMed. The interannual variability in salinity was associated with the reversal of the NIG circulation. During the anticyclonic phases of the NIG (figure 1(b)), the inflow of fresh AW in the CMed led to decreased mean salinity values in both the surface and intermediate layers (gray shaded periods in figures 2(a) and (b)). Conversely, during the cyclonic phases of the NIG (figure 1(c)), the inflow of LSW and LIW led to high salinity values in the surface and intermediate layers (yellow-shaded periods in figures 2(a) and (b)). This condition is more pronounced in the South Adriatic region, where all the data considered were located within the SAG. In contrast, in the Ionian Sea, to maintain temporal continuity, the data were considered over a larger area (indicated by the large magenta box in figure 1(a)) and were not limited to the region specifically showing the signature of the NIG (the small red box in figure 1(a)).

Figure 2(c) shows the surface salinity distribution in the CMed in 2011, before the salinification process started, and ten years later in 2021. The upper layers of the North Ionian and South Adriatic became much saltier during that decade, with surface salinities exceeding 39 psu. This sharp increase in salinity was related to

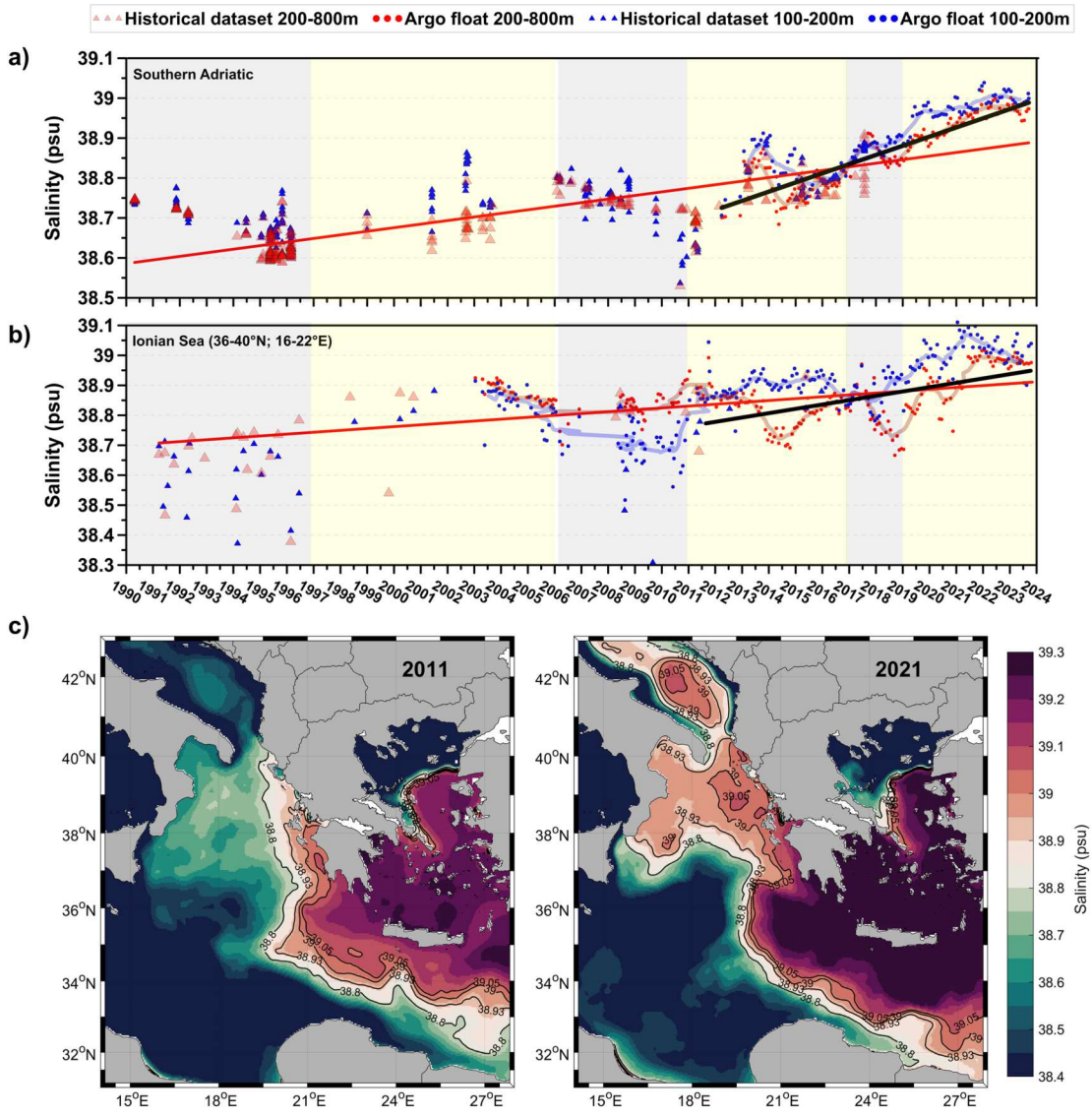

Figure 2. Time-series of salinity in the Southern Adriatic (a) and Ionian (b) seas in the upper (100–200 m; blue) and intermediate (200–800 m; red) layers; grey and yellow shaded areas highlight the anticyclonic and cyclonic NIG circulation modes, respectively; red and black continuous lines are the salinity trends from 1990 and from 2012, respectively, in the intermediate layers. (c) Yearly surface salinity patterns at 3 m depth in 2011 (left) and 2021 (right).

the inflow of salty water from the Aegean and Levantine Basins. These waters were transported northward from the Cretan Passage or the western Cretan straits along the eastern Ionian coast, spread in the North Ionian sector, and reached the South Adriatic. The coastal pathway along the Greek coast represents a direct link between the Levantine/Aegean basins and SAG (Mihanović *et al* 2021, Menna *et al* 2021, 2022b). Following the path of this coastal circuit, surface and intermediate waters moved from the Levantine towards the southern Ionian along the southern Cretan coast, recirculated in the Pelops Gyre, where they also collected Aegean waters, from which they were redirected northward towards the North Ionian and Adriatic Seas.

Vorticity fields were computed within the small red box in the North Ionian and the red-circled area in the South Adriatic area, as highlighted in figure 1(a). NIG inversions were characterized by decreasing or even negative vorticity values during anticyclonic modes and positive values during cyclonic modes (figure 3(a), red curve, left axis). In contrast, the SAG showed greater vorticity magnitudes and a broader range than the North Ionian region, with consistently positive values throughout the time series (figure 3(a), black curve, right-hand axis). This behavior reflects the permanent cyclonic circulation of SAG (see the insert of figure 1(a)). Despite its persistent cyclonic circulation, the strength of the SAG responded to NIG reversals; cyclonic vorticity increased following NIG anticyclonic modes (e.g., 2013–2014, 2018, and 2023) and decreased after NIG cyclonic modes (e.g., 2011–2012, 2016–2017, and 2020–2021).

The vorticity field was primarily controlled by three terms in the vorticity equation: wind stress, horizontal advection, and baroclinicity (figure 3(b) and table 1). Despite their interannual variability, all three

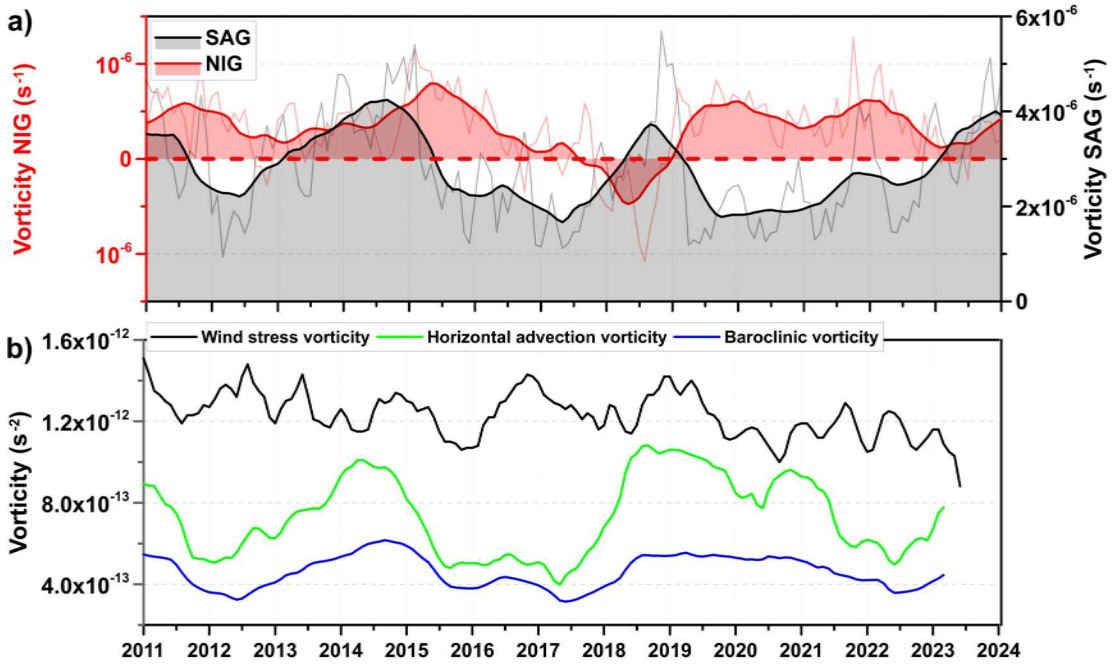

Figure 3. (a) Time series of the spatially averaged current vorticity (light red and grey lines) and low-pass filtered (13 months) current vorticity (red and black lines) computed in the NIG and SAG subregions (highlighted in red in figure 1). Time series of the (b) wind stress curl term of the vorticity equation computed in the SAG.

Table 1. (left) Mean contribution to the vorticity field for the different terms of the vorticity equation: wind stress (ws), horizontal advection (adv) and baroclinic (bar). (right) Correlation coefficients (95% confidence level) between the time series of the relative vorticity and those of the different terms of vorticity equation.

Mean vorticity terms (2011–2023)			Vorticity cross correlation 2011–2023			
ws	adv	bar	ζ versus curl(τ)	ζ versus adv	ζ versus bar	ζ versus adv+bar
1.2×10^{-12}	0.8×10^{-12}	0.5×10^{-12}	0.16	0.53	0.60	0.60

contributions were consistently cyclonic (positive) and of the same order of magnitude (10^{-12} s^{-2}). Wind stress had the highest absolute values and exhibited a decreasing trend since 2011. In contrast, the horizontal advection and baroclinic terms exhibited stronger temporal fluctuations, with pronounced peaks in 2014, 2018, and 2023, which coincided with the peaks in the relative vorticity time series. Combined, the horizontal advection and baroclinic contributions accounted for the absolute value in the relative vorticity field similar to that induced by wind stress.

Cross-correlations were calculated between the time series of the relative vorticity of the current field and the different terms of the vorticity equation (wind stress, horizontal advection, and baroclinicity) considered separately, and for the sum of the advection and baroclinicity terms (table 1). The correlation coefficients presented in this paper are statistically significant ($p < 0.05$, the probability that the null hypothesis is true, i.e., no correlation is lower than 5%; confidence level 95%). The correlations exceeding 0.5 for both the baroclinic and horizontal advection terms were considered separately or combined, whereas the wind stress term showed a statistically significant but weak correlation. The baroclinic term, associated with density gradients, exerted stronger control over the temporal variability of relative vorticity during 2011–2023, as indicated by a correlation coefficient of 0.6 (table 1).

The vorticity peaks in the SAG in 2014 and 2018 were associated with the strengthening of the northward meridional transport along the eastern (positive values, northward direction; green curve in figure 4(a)) and western (negative values, southward direction; purple line in figure 4(a)) edges of the SAG in the surface layer. These waters are relatively less saline and of Atlantic origin (figure 4(b)). Conversely, the reduction in vorticity was related to weaker meridional transport along the edges of the SAG, with relatively more saline water of Levantine origin filling the South Adriatic (figures 4(a) and (b)). The salinity oscillations observed in the SAG mirror those of the North Ionian (figure 4(b)), suggesting that water mass exchange with neighbouring areas is the main cause of the salinity distribution in the South Adriatic (the cross-correlation coefficient between the salinity time series in the SAG and North Ionian is 0.78; $p < 0.05$; confidence level 95%). The temperature

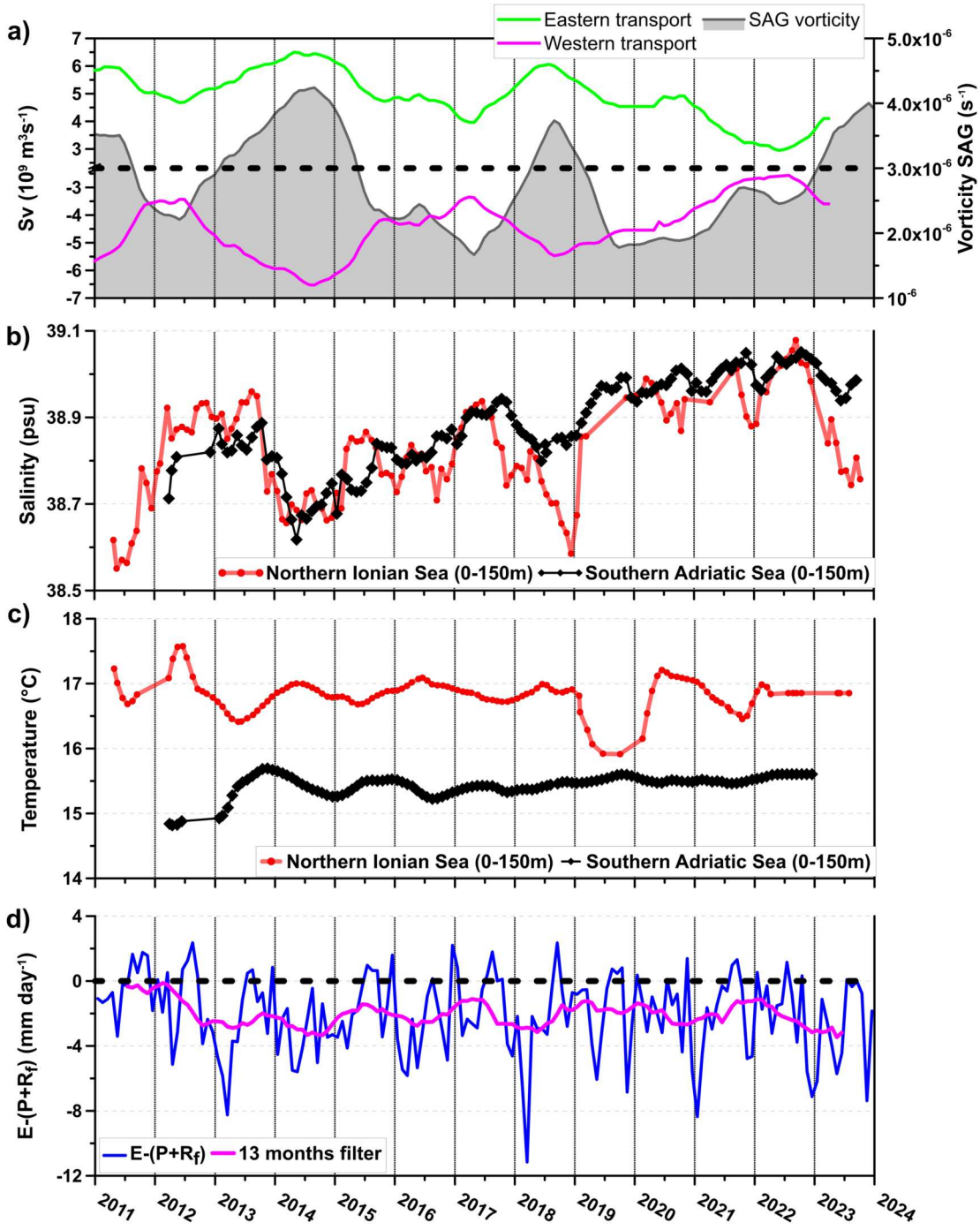

Figure 4. Time-series of the meridional components of the volume transport in the surface layer (a) across the eastern (green) and the western (purple) transects of the SAG superimposed on the time series of the spatially averaged low-pass filtered current vorticity (black curve and grey shaded area) in the SAG sub-region. The geographical location of the transect is shown in figure 1(a). Monthly time series of salinity (b) and of the low-pass filtered (13 months) temperature (c) derived from Argo float in the NIG (red) and SAG (black) subregions defined in figure 1(a). Monthly time series (d) of freshwater fluxes (blue) and low-pass filtered (13 months) freshwater fluxes (pink) derived from ERA5 products in the SAG.

fluctuations in the SAG (figure 4(c)) showed a slightly positive trend in the SAG and no-trend in the Ionian, but no interannual variability was consistent with the vorticity variations (non-significant cross-correlation between the two variables).

Local forcing, such as freshwater flux, which displays high seasonal variability (blue curve, figure 4(d)), can also contribute to salinity changes. River runoff makes the Adriatic Sea a dilution basin (Cushman-Roisin *et al* 2008, Verri *et al* 2024), characterized by negative freshwater flux values throughout the entire time series considered (P+Rf outweighs E; figure 4(d)). Sensitivity studies have shown that rivers significantly influence the seasonal variability of thermohaline circulation, dynamics, and stratification of the Adriatic Sea (e.g. Vilibić *et al* 2016, Vodopivec *et al* 2022). However, although the variability of freshwater flux is not negligible, its

interannual fluctuations do not appear to be linked to changes in salinity in the SAG, as there is no significant cross-correlation between the monthly time series of salinity and freshwater fluxes. Local freshwater fluxes in the SAG exerted less influence than horizontal advection from the North Ionian in determining the interannual variability of salinity in the SAG. This finding contrasts with the conclusions by Terzić *et al* (2025). While these authors attributed salinity changes in the deep layer of the SAP to local processes based on a 10-year comparison with the deep layer of the northeastern Ionian Sea, our results suggest that this explanation is incomplete. The SAP and North Ionian Sea are closely coupled at the surface (figure 4(b)), and this variability can propagate to deeper layers through convective processes.

Taken together, these results suggest that horizontal advection and baroclinic terms interacted to cause fluctuations in vorticity in the upper layer (0–150 m depth) of the SAG. The baroclinic contribution is related to the density gradients, which are predominantly controlled by salinity. Salinity variability is predominantly controlled by advection from the Ionian Sea rather than by local processes. To further examine this mechanism, we performed high-resolution analysis using glider observations. A cyclonic gyre is typically characterized by a higher density and lower temperatures at its center compared to its edge, resulting in a persistent density gradient from the center to the periphery. This condition creates a pressure gradient force ($\mathbf{F}_p$) directed towards the center of the gyre (figure 5, upper panels), which helps sustain the cyclonic circulation field along the edges of the structure. *Insitu* data collected by ocean gliders across the SAG (Bari–Dubrovnik transect; inset of figure 1(a)) help us to understand how the vertical density structure of the area changes during a period of maximum positive vorticity (16–22 February 2014) compared to a period of minimum positive vorticity (20–26 November 2015). From 2012 onwards, the SAG core was filled with high-salinity water (figure 2(c)). Under these conditions, the inflow of fresher waters along the eastern flank of the SAP and their subsequent cyclonic recirculation along the margins of the gyre enhanced the center-to- edge salinity and, in turn, the density gradients in the upper layer (figure 5(a)).

The doming of the isopycnals indicated upwelling in the center of the SAG and downwelling along its flanks (figure 5(a)), and the shape of the isopycnals was closely related to the vertical salinity structure. This increased the salinity-driven component of the pressure gradient force (F_{ps}) towards the gyre center, providing an additional positive contribution to the circulation field and resulting in vorticity maxima in the SAP. Conversely, during periods when saltier waters of Levantine origin intruded along the edge of the SAG, the center-to-edge density gradient weakened (figure 5(b)), reducing $\mathbf{F}_{ps}$. The isopycnals showed a slight downward curvature in the center of the gyre, and their shape mirrored the salinity distribution (figure 5(b)). The thermohaline structure of the water column subtracts the positive vorticity from the mean field, weakening the cyclonic signature of the SAP. Overall, the contrasting density structures and isopycnal shapes observed in the two periods are consistent with the observed salinity variability.

High-resolution analyses based on glider data highlight the role of salinity in modulating vorticity, and consequently, the current field in the surface layer of the SAG. Although this analysis covers only short time periods, it reveals dynamics that can be conceptually extended to the entire observation period (2011–2023) using MEDSEA products. Therefore, to describe the influence of thermohaline conditions on the vorticity field, we determined the annual temperature and salinity differences between the center and the western and eastern edges of the SAG along a transect zonally crossing the gyre (figure 1(a)). The eastern edge was consistently warmer than the center (green curve, figure 5(c)), increasing the pressure gradient force between the edge and center of the gyre, which, in turn, increased the positive vorticity of the area. The positive temperature contribution to the vorticity field peaked in 2015 and reached a minimum in 2018 (green curve, figure 5(c)). The western edge was periodically affected by cold water advection from the North Adriatic, sometimes making it warmer (2011, 2013, 2019–2023) and sometimes colder (2012, 2014–2018) than the center (purple curve, figure 4(c)). In conclusion, when the difference between the center and edge of the SAG was negative, the temperature contributed positively to the vorticity field, whereas when this difference was positive, the pressure gradient between the edge and center decreased, thereby reducing the positive vorticity from the SAG. The time series of the temperature differences showed no clear relationship with the vorticity field evolution (figure 5(c)). In terms of salinity differences, the two edges of the SAG behaved very similarly, and the center of the gyre was always saltier than the edges (figure 5(d)). The salinity difference over time (green and purple curves in figure 5(d)) exhibited fluctuations similar to those in the vorticity time series, with peaks aligned with the maximum values of the vorticity field. The high salinity difference on the western edge of the SAG observed in 2017 (figure 5(d)) was linked to the inflow of NAdDW and strong open ocean convection that occurred that year (Kokkini *et al* 2020, Mihanović *et al* 2021, Martellucci *et al* 2025).

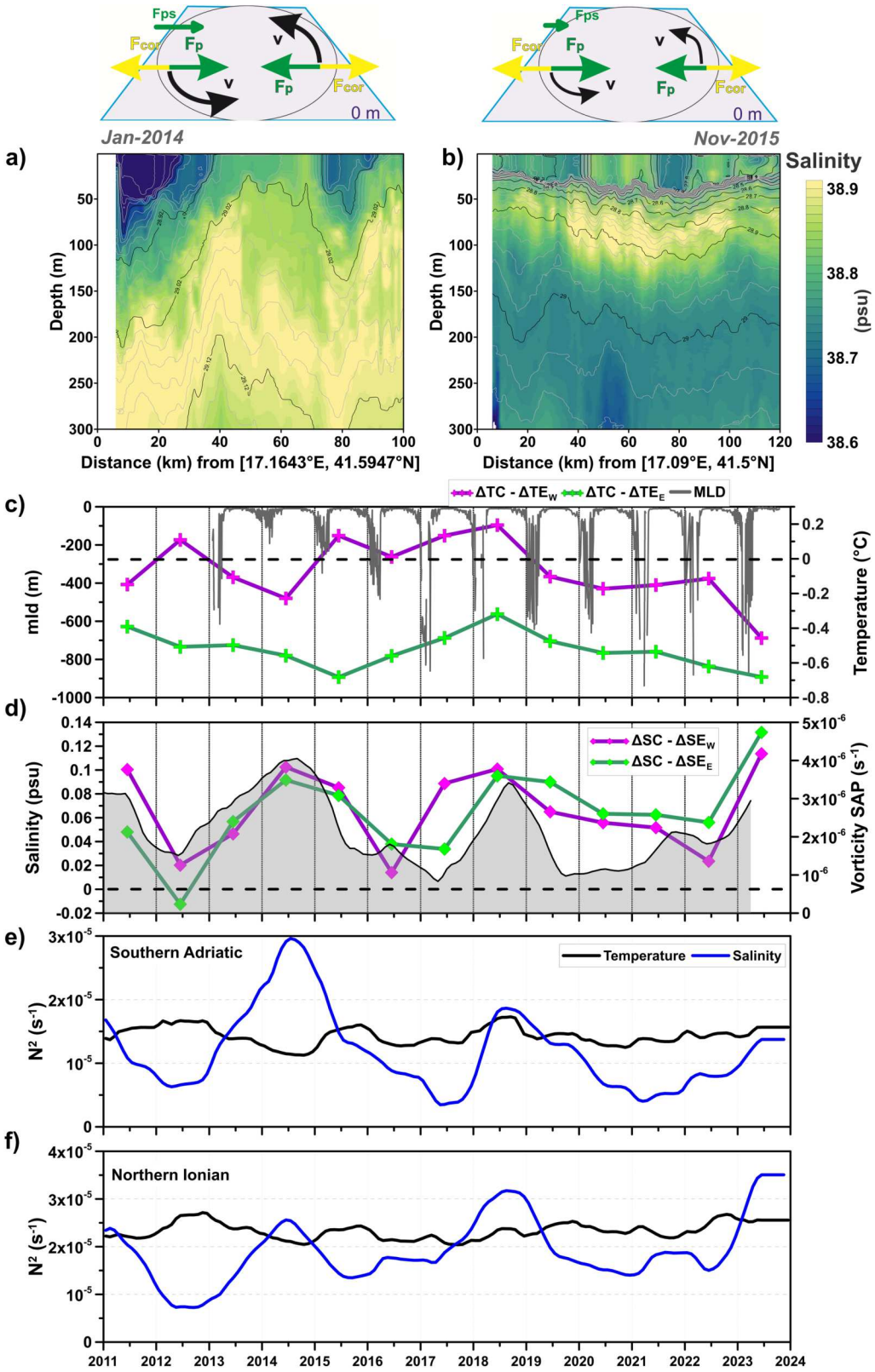

Figure 5. Contour diagram of salinity along two glider sections (Bari-Dubrovnik) carried out in (a) February 2014 (Convex 14 in figure 1(a)) and (b) November 2015 (Pre-Convex 2016 in figure 1(a)) as function of depth and distance from the starting point Ba (figure a1). Black contours lines are the isopycnals. Time-series of yearly temperature (c) and salinity (d) differences between the center and the eastern (green), and the western (purple) edges of the SAG in the 0–150 m layer. The geographical location of centre and edges is shown in figure 1(a). Time-series of temperature differences in (c) are superimposed on the monthly time-series of the float derived MLD (grey line). Time-series of salinity differences in (d) are superimposed on the time-series of the spatially averaged low-pass filtered current vorticity in the SAG sub-region (black curve and grey shaded area). Time-series to the Brunt-Väisälä frequency (N^2) of contributions from the temperature (black) and salinity (blue) in the SAG (e) and NIG (f) subregions in the layer 0–150 m.

Discussion and conclusions

In an era marked by ocean warming, increased stratification trends, and decreased upper-layer density, salinity plays a crucial role in determining the density structure of the water column and in shaping its thermohaline variability. This has direct implications for the surface current field and stability of the water column. However, the specific impact of salinity on surface currents is not well understood, particularly with regard to its effect on thermohaline processes (Chen *et al* 2021).

In the CMed, which has experienced positive temperature trends and steeper salinification over the last decade (Pastor *et al* 2020, Kubin *et al* 2023, Terzić *et al* 2025), salinity has emerged as a critical factor influencing ocean dynamics. The anticyclonic phases of the NIG have weakened over the past decade, with shorter durations and lower intensities than those observed in the 1990s (Mihanović *et al* 2021, Menna *et al* 2022b, Civitarese *et al* 2023). While the 1990s anticyclonic inversion persisted for almost ten years, the subsequent inversion from 2006 to 2010 lasted only approximately five years. After 2011, during the period analyzed in this study, anticyclonic phases became markedly shorter, typically lasting only one–two years. The frequent NIG reversals observed after 2011 corresponded with the marked variability in the strength of the vorticity field in the SAG. Both phenomena appear to be strongly influenced by progressive salinification of the upper layer of the CMed.

However, the key factors influencing the temporal variability of the vorticity field in the CMed after 2011 were the horizontal advection and baroclinic instability of the water column. The importance of the first baroclinic mode and advection in shaping the horizontal circulation of the North Ionian was described in detail by Eusebi Borzelli *et al* (2024) and Napolitano *et al* (2025), respectively. Here, we also added a direct connection between these two forcings and the South Adriatic. The variability of horizontal advection due to the inflow/outflow of different water masses contributed to shaping the variability of the vorticity field in the period 2011–2023 in the SAG (figure 3(b); table 1). The inflow of AW was associated with the enhancement of meridional transport along both the eastern and western edges of the gyre, whereas the inflow of LSW was characterized by a lower meridional transport (figure 4(a)). The contribution of vorticity advection was particularly pronounced during the anticyclonic phases of the NIG, which is consistent with the findings of Shabrang *et al* (2016).

The deflection of the AW along the western edge of the North Ionian and around the periphery of the SAG caused by the anticyclonic NIG increased the salinity gradient from the center to the edge of these gyres (figure 5(d)). This resulted in a positive (cyclonic) contribution to the vorticity field during 2013–2014, 2018, and 2023. While this positive contribution increased the vorticity of the SAG, it also reduced the temporal extent and intensity of the recent NIG anticyclonic phases, thereby adding a positive contribution to the vorticity field.

The alternating inflow of AW and LSW along the periphery of the SAG and NIG subregions played a crucial role in determining water column stability in the CMed. The contribution of temperature to water column stability was comparable in magnitude to that of salinity on an interannual scale, but salinity showed much more pronounced interannual variability in both the SAG and NIG subregions (figures 5(e), (f)). The inflow of AW notably enhanced the contribution of salinity to water column stability, peaking during years characterized by the strengthening of the vorticity field in the SAG (2014 and 2018, figures 4(d)–(f)). Under these conditions, the contribution of salinity outweighed that of temperature, especially during 2014–2015 in the SAG (figure 4(e)) and 2017–2018 in the NIG (figure 4(f)). The inflow of LSW reduced the salinity contribution to the stability of the water column, with minima marked in years characterized by the weakening of the vorticity field in the SAG (2012, 2015–2017, 2019–2022, figures 5(d)–(f)). This reduction in the stability of the water column most likely made it more prone to deep convection phenomena, which occurred in years with LSW inflow (e.g. 2017, 2021–2023) and were reduced in the years with AW inflow (e.g. 2014–2015) in the SAG (figure 5(c)).

In Terzić *et al* (2025), the authors argue that the recent warming and salinification observed in the bottom layer of the SAP are primarily driven by local processes, rather than advection from the North Ionian Sea. However, this conclusion is based on a limited number of Argo float profiles, sampled only along the northeastern Ionian margin. In contrast, the results presented here are derived from a substantially larger, more comprehensive dataset that encompasses the entire North Ionian region. These results demonstrate that salinity variations in the South Adriatic closely mirror that in the North Ionian region within the 0–150 m layer (figure 4(b)). This establishes a robust, basin-scale connection between the two regions. As the hydrographic properties of the upper layer strongly influence the vertical stability of the water column and modulate winter convection, variability in the surface layer can propagate downwards and affect the deep waters of the SAP. Therefore, changes in the deep layer observed in the South Adriatic are dynamically linked to the state of the upper layer, which is in turn closely connected to the variability in the North Ionian.

This study integrates *in situ* observations, satellite data and model reanalyses to assess salinity-driven dynamics. However, each dataset has inherent limitations: gliders provide high-resolution vertical profiles but limited coverage; Argo floats offer broader temporal sampling but coarser vertical resolution; satellites mainly

capture surface properties, missing critical subsurface processes for dense water formation; although model reanalyses are valuable for filling observational gaps, they include approximations that can affect the representation of salinity effects. Despite these uncertainties, the combined approach provides a robust assessment of salinity-driven dynamics in the CMed. This highlights the area's growing role in circulation and thermohaline variability, offering insights that could be applied to similar processes in other regions of the global ocean.

Our results highlight the central role of salinity in driving the dynamics of the CMed. Salinity is not merely a passive tracer; as a fundamental oceanic state variable, it governs density, stratification and, ultimately, the behaviour of many regional circulation features. Since 2012, the CMed has experienced a significant and sustained increase in salinity, primarily due to the increased inflow of salt-rich waters from the Aegean and Levantine basins. This trend has increased the dynamic influence of salinity on the system. In particular, we find that salinity variations strongly modulate vorticity in the SAG. During periods of intensified AW inflow, horizontal gradients steepen, and the gyre's cyclonic vorticity is reinforced; through this mechanism, salinity increasingly controls the water-column stability. Overall, these findings demonstrate that salinity is a primary regulator of the thermohaline variability in the CMed, shaping the vertical structure of the water column and the large-scale surface circulation field. Consequently, understanding and monitoring salinity changes is essential for predicting the future evolution of the thermohaline circulation in the Mediterranean and its basin-scale impacts.

Acknowledgments

This research was funded by the Italian Ministry of University and Research as part of the ARGO-ITALY program. Argo float data were collected and made freely available by the International Argo Program and the national programs that contribute to it (https://argo.ucsd.edu, https://www.ocean-ops.org). The Argo Program is a part of the Global Ocean Observing System.

Conflict of interest declaration

The authors declare that they have no affiliations with or involvement in any organization or entity with any financial interest in the subject matter or materials discussed in this manuscript.

Data availability statement

The data that support the findings of this study are openly available at the following URL/DOI: https://argo.ucsd.edu, https://www.ocean-ops.org.

Ethical compliance

This article does not contain any studies involving human participants performed by any of the authors.

Author contributions

Milena Menna 0000-0002-0149-0502
Conceptualization (lead), Data curation (equal), Investigation (lead), Methodology (equal), Writing – original draft (lead), Writing – review & editing (lead)

Miroslav Gačić
Conceptualization (equal), Investigation (supporting)

Annunziata Pirro
Data curation (equal), Validation (equal), Writing – review & editing (equal)

Elena Mauri 0000-0001-9602-0628
Funding acquisition (equal), Supervision (equal), Writing – review & editing (equal)

Gilda Savonitto 0000-0001-5893-3143
Validation (equal), Visualization (equal), Writing – review & editing (equal)

Massimo Pacciaroni 0000-0001-6397-8717
Data curation (equal), Software (equal), Writing – review & editing (equal)

Vanessa Cardin 0000-0002-4710-6844
Supervision (equal), Writing – review & editing (equal)

Giulio Notarstefano 0000-0002-8532-2097
Validation (equal), Writing – review & editing (equal)

Antonella Gallo 0000-0002-8836-1550
Data curation (equal), Writing – review & editing (supporting)

Piero Zuppelli
Data curation (supporting), Writing – review & editing (equal)

Antonio Bussani 0000-0003-0340-3078
Software (equal), Writing – review & editing (equal)

Riccardo Martellucci 0000-0001-7859-3967
Conceptualization (equal), Data curation (equal), Investigation (equal), Software (equal), Writing – original draft (equal), Writing – review & editing (equal)

References

Amorim F L, Le Meur J, Wirth A and Cardin V 2024 Tipping of the double-diffusive regime in the southern Adriatic Pit in 2017 in connection with record high-salinity values *Ocean Sci.* **20** 463–74
Argo 2020 *Float Data and Metadata from Global Data Assembly Centre (Argo GDAC)* (SEANOE) https://doi.org/10.17882/42182
Bensi M, Cardin V, Rubino A, Notarstefano G and Poulain P M 2013 Effects of winter convection on the deep layer of the Southern Adriatic Sea in 2012 *J. Geophys. Res. Oceans* **118** 6064–75
Bensi M, Velaoras D, Meccia V L and Cardin V 2016 Effects of the Eastern Mediterranean Sea circulation on the thermohaline properties as recorded by fixed deep-ocean observatories *Deep Sea Res. Pt I* **112** 1–13
Bessières L, Rio M H, Dufau C, Boone C and Pujol M I 2013 Ocean state indicators from MyOcean altimeter products *Ocean Sci.* **9** 545–60
Böhme L and Send U 2005 Objective analyses of hydrographic data for referencing profiling float salinities in highly variable environments *Deep Sea Res. Pt II* **52** 651–64
Cabanes C *et al* 2021 DMQC cookbook for core Argo parameters *Ifremer* **1** 1–77
Cabanes C, Thierry V and Lagadec C 2016 Improvement of bias detection in Argo float conductivity sensors and its application in the North Atlantic *Deep Sea Res. Pt I* **114** 128–36
Cardin V, Wirth A, Khosravi M and Gačić M 2020 South adriatic recipes: estimating the vertical mixing in the deep Pit *Front. Mar. Sci.* **7** 565982
Cheng L J and Coauthors 2021 Upper ocean temperatures hit record high in 2020 *Adv. Atmos. Sci.* **38** 523–30
Civitarese G, Gačić M, Batistić M, Bensi M, Cardin V, Dulčić J, Garić R and Menna M 2023 The BiOS mechanism: history, theory, implications *Prog. Oceanogr.* **216** 103056
Cushman-Roisin B, Gualtieri C and Mihailović D T 2008 Environmental fluid mechanics: current issues and future outlook *Fluid Mechanics of Environmental Interfaces* (Taylor & Francis) https://doi.org/10.4324/9780203895351-6
Di Biagio V, Martellucci R, Menna M, Teruzzi A, Amadio C, Mauri E and Cossarini G 2023 Dissolved oxygen as an indicator of multiple drivers of the marine ecosystem: the southern Adriatic Sea case study *7th edition of the Copernicus Ocean State Report (OSR7)* vol 1 ed K von Schuckmann *et al* (Copernicus Publications) pp 1–13
England M 1995 The age of water and ventilation timescales in a global ocean model *J. Phys. Oceanogr.* **25** 2756–77
Escudier R *et al* 2020 Mediterranean sea physical reanalysis (CMEMS MED-Currents) *Version 1 [Data Set] (Copernicus Monitoring Environment Marine Service (CMEMS) publishing)* **2.5** 1–67
Eusebi Borzelli G L and Carniel S 2023 A reconciling vision of the Adriatic-Ionian bimodal oscillating system *Sci. Rep.* **13** 2334
Eusebi Borzelli G L, Napolitano E, Carillo A, Struglia M V, Palma M and Iacono R 2024 Hydrographic versus dynamic description of a basin: the example of baroclinic motion in the Ionian Sea *Oceans* **5** 383–97
Eusebi Borzelli G L, Napolitano E, Iacono R and Struglia M V 2025 Decadal trends in buoyancy, internal modes and horizontal dynamics in the Northern Ionian *Sea Oceans* **6** 69
Gačić M, Civitarese G, Eusebi Borzelli G L, Kovačević V, Poulain P M, Theocharis A, Menna M, Catucci A and Zarokanellos N 2011 On the relationship between the decadal oscillations of the northern Ionian Sea and the salinity distributions in the eastern Mediterranean *J. Geophys. Res. Oceans* **116** 2–5
Gačić M *et al* 2014 Extreme winter 2012 in the Adriatic: an example of climatic effect on the BiOS rhythm *Ocean Sci.* **10** 513–22
Gačić, Eusebi M, Borzelli, G L, Civitarese G, Cardin V and Yari S 2010 Can internal processes sustain reversals of the ocean upper circulation? The Ionian Sea example *Geophys. Res. Lett.* **37** 2–5L09608
Gačić M, Civitarese G, Miserocchi S, Cardin V, Crise A and Mauri E 2002 The open-ocean convection in the Southern Adriatic: a controlling mechanism of the spring phytoplankton bloom *Cont. Shelf Res.* **22** 1897–908
Gačić M, Schroeder K, Civitarese G, Cosoli S, Vetrano A and Eusebi Borzelli G L 2013 Salinity in the Sicily Channel corroborates the role of the Adriatic–Ionian Bimodal Oscillating System (BiOS) in shaping the decadal variability of the Mediterranean overturning circulation *Ocean Sci.* **9** 83–90

Gačić M *et al* 2021 Impact of the dense water flow over the sloping bottom on the open-sea circulation: Laboratory experiments and the Ionian Sea (Mediterranean) example *Ocean Sci. Discuss.* **17** 975–96
Hersbach H *et al* 2020 The ERA5 global reanalysis *Q. J. R. Meteorol. Soc.* **146** 1999–2049
Hu A, Meehl G A, Han W, Lu J and Strand W G 2013 Energy balance in a warm world without the ocean conveyor belt and sea ice *Geophys. Res. Lett.* **40** 6242–6
IOC, SCOR and IAPSO 2010 The international thermodynamic equation of seawater—2010: calculation and use of thermodynamic properties *Intergovernmental Oceanographic Commission, Manuals and Guides No. 56* (UNESCO) 196
Kassis D and Korres G 2021 Recent hydrological status of the Aegean Sea derived from free drifting profilers *Mediterr. Mar. Sci.* **22** 347–61
Kokkini Z, Mauri E, Gerin R, Poulain P M, Simoncelli S and Notarstefano G 2020 On the salinity structure in the South Adriatic as derived from float and glider observations in 2013–2016 *Deep Sea Res. Pt II* **171** 104625
Kubin E, Menna M, Mauri E, Notarstefano G, Mieruch S and Poulain P M 2023 Heat content and temperature trends in the Mediterranean Sea as derived from Argo float data *Front. Mar. Sci.* **10** 1271638
Le Meur J, Wirth A, Paladini de Mendoza F, Miserocchi S and Cardin V 2025 Intermittent supply of dense water to the deep South Adriatic Pit: an observational study *Front. Mar. Sci.* **12** 1516780
Li G, Cheng L, Zhu J, Trenberth K E, Mann M E and Abraham J P 2020 Increasing ocean stratification over the past half-century *Nat. Clim. Chang.* **10** 1116–23
Lipizer M, Partescano E, Rabitti A, Giorgetti A and Crise A 2014 Qualified temperature, salinity and dissolved oxygen climatologies in a changing Adriatic *Sea Ocean Sci.* **10** 771–97
Manca B B, Budillon G, Scarazzato P and Ursella L 2003 Evolution of dynamics in the eastern Mediterranean affecting water mass structures and properties in the Ionian and Adriatic Seas *J. Geophys. Res. Oceans* **108** C9
Manca B B, Ursella L and Scarazzato P 2002 New development of Eastern Mediterranean circulation based on hydrological observations and current measurements *Mar. Ecol.* **23** 237–57
Mantziafou A and Lascaratos A 2004 An eddy resolving numerical study of the general circulation and deep-water formation in the Adriatic Sea *Deep Sea Res. Pt I* **51** 921–52
Martellucci R *et al* 2024 Recent changes of the dissolved oxygen distribution in the deep convection cell of the southern Adriatic Sea *J. Mar. Syst.* **245** 103988
Martellucci R *et al* 2025 A multiobservation analysis of the 2017 dense water formation events: Climate change, bottom density currents, and Adriatic-Ionian sea circulation (Mediterranean Sea) *J. Geophys. Res. Oceans* **130** e2024JC022306
Meli M, Camargo C M L, Olivieri M, Slangen A B A and Romagnoli C 2023 Sealevel trend variability in the Mediterranean during the 1993–2019 period *Front. Mar. Sci.* **10** 1150488
Meli M 2024 The potential recording of North Ionian Gyre's reversals as a decadal signal in sea level during the instrumental period *Sci. Rep.* **14** 4907
Menna M, Gačić M, Martellucci R, Notarstefano G, Fedele G, Mauri E, Gerin R and Poulain P M 2022a Climatic, decadal, and interannual variability in the upper layer of the Mediterranean Sea using remotely sensed and *in situ* data *Remote Sens.* **14** 1322
Menna M, Martellucci R, Notarstefano G, Mauri E, Gerin R, Pacciaroni M, Bussani A, Pirro A and Poulain P M 2022b Record-breaking high salinity in the South Adriatic Pit in 2020 2022b *Copernicus Marine Service Ocean State Report (Issue 6)* vol 15 ed K von Schuckmann *et al* (Taylor & Francis Publishing) pp s199–205
Menna M, Gerin R, Notarstefano G, Mauri E, Bussani A, Pacciaroni M and Poulain P M 2021 On the circulation and thermohaline properties of the Eastern Mediterranean Sea *Front. Mar. Sci.* **8** 671469
Menna M *et al* 2023 A case study of impacts of an extreme weather system on the Mediterranean Sea circulation features: Medicane Apollo (2021) *Sci. Rep.* **13** 3870
Menna M and Poulain P M 2010 Mediterranean intermediate circulation estimated from Argo data in 2003–2010 *Ocean Sci.* **6** 331–43
Menna M, Reyes Suarez N C, Civitarese G, Gačić M, Rubino A and Poulain P M 2019 Decadal variations of circulation in the Central Mediterranean and its interactions with the mesoscale gyres *Deep Sea Res. Pt II* **164** 14–24
Mihanović H, Vilibić I, Šepić J, Matić F, Ljubešić Z, Mauri E, Gerin R, Notarstefano G and Poulain P M 2021 Observation, preconditioning and recurrence of exceptionally high salinities in the Adriatic Sea *Front Mar. Sci.* **8** 672210
Napolitano E, Carillo A, Struglia M V, Iacono R, Palma M, Eusebi Borzelli G L and Sannino G 2025 The role of the Atlantic-Ionian stream in the long-term variability of the surface circulation in the Northern Ionian Sea: Results from a hindcast simulation *Prog. Oceanogr.* **234** 103472
Notarstefano G, Menna M and Legeais J-F 2019 Reversal of the Northern Ionian circulation in 2017. 2019 *Copernicus Marine Service Ocean State Report (Issue 3)* vol 12 ed K von Schuckmann *et al* (Taylor & Francis Publishing) pp s108–11
Notarstefano G and Poulain P M 2013 *Delayed mode quality control of Argo salinity data in the Mediterranean Sea: a regional approach* Report 2013/103 Sect. OCE 40 MAOS Istituto Nazionale di Oceanografia e di Geofisica Sperimentale
O'Hare G 2011 Updating our understanding of climate change in the North Atlantic: the role of global warming and the Gulf Stream *Geogr* **96** 5–15
Ozer T, Rahav E, Gertman I, Sisma-Ventura G, Silverman J and Herut B 2022 Relationship between thermohaline and biochemical patterns in the levantine upper and intermediate water masses, Southeastern Mediterranean Sea (2013–2021) *Front. Mar. Sci.* **9** 958924
Owens W B and Wong A P S 2009 An improved calibration method for the drift of the conductivity sensor on autonomous CTD profiling floats by θ–S climatology *Deep Sea Res. Pt I* **56** 450–7
Paladini de Mendoza F, Schroeder K, Langone L, Chiggiato J, Borghini M, Giordano P and Miserocchi S 2023 Deep-water dynamics along the 2012–2020 observations on the continental margin of the Southern Adriatic Sea (Mediterranean Sea) *J. Mar. Sci. Eng.* **11** 1364
Pastor F, Valiente J A and Khodayar S 2020 A warming Mediterranean: 38 years of increasing sea surface temperature *Remote Sens.* **12** 2687
Pinardi N, Cessi P, Borile F and Wolfe C L 2019 The Mediterranean sea overturning circulation *J. Phys. Oceanogr.* **49** 1699–721
Pinardi N *et al* 2015 Mediterranean Sea large-scale low-frequency ocean variability and water mass formation rates from 1987 to 2007: a retrospective analysis *Prog. Oceanogr.* **132** 318–32
Pirro A, Mauri E, Gerin R, Martellucci R, Zuppelli P and Poulain P M 2022 New insights on the formation and breaking mechanism of convective cyclonic cones in the South Adriatic Pit during winter 2018 *J. Phys. Oceanogr.* **52** 2049–68
Pirro A *et al* 2024 Rossby waves driven by the Mid Mediterranean Jet impact the Eastern Mediterranean mesoscale dynamics *Sci. Rep.* **14** 29598
Placenti F, Torri M, Pessini F, Patti B, Tancredi V, Cuttitta A, Giaramita L, Tranchida G and Sorgente R 2022 Hydrological and biogeochemical patterns in the Sicily channel: new insights from the last decade (2010-2020) *Front. Mar. Sci.* **9** 733540

Poulain P M and Cushman-Roisin B 2001 Circulation *Physical Oceanography of the Adriatic Sea: Past, Present and Future* ed B Cushman-Roisin *et al* (Kluwer Academic Publishing) pp 67–109
Poulain P M, Menna M and Mauri E 2012 Surface geostrophic circulation of the Mediterranean Sea derived from drifter and satellite altimeter data *J. Phys. Oceanogr.* **42** 973–90
Pranić P, Denamiel C, Janeković I and Vilibić I 2023 Multi-model analysis of the Adriatic dense-water dynamics *Ocean Sci.* **19** 649–70
Reale M, Salon S, Crise A, Farneti R, Mosetti R and Sannino G 2017 Unexpected covariant behavior of the Aegean and Ionian Seas in the period 1987–2008 by means of a nondimensional sea surface height index *J. Geophys. Res. Oceans* **122** 8020–33
Rio M H, Pascual A, Poulain P M, Menna M, Barceló B and Tintoré J 2014 Computation of a new mean dynamic topography for the Mediterranean Sea from model outputs, altimeter measurements and oceanographic *in situ* data *Ocean Sci.* **10** 731–44
Schroeder K, Chiggiato J, Josey S A, Borghini M, Aracri S and Sparnocchia S 2017 Rapid response to climate change in a marginal sea *Sci. Rep.* **7** 4065
Schroeder K, Cozzi S, Belgacem M, Borghini M, Cantoni C, Durante S, Petrizzo A, Poiana A and Chiggiato J 2020 Along-path evolution of biogeochemical and carbonate system properties in the intermediate water of the Western Mediterranean *Front. Mar. Sci.* **7** 375
Schroeder K *et al* 2024 A consensus-based, revised and comprehensive catalogue for Mediterranean water masses acronyms *Mediterr. Mar. Sci.* **25** 783–91
Schneider A, Tanhua T, Kortzinger A and Wallace D W R 2010 High anthropogenic carbon content in the eastern Mediterranean *J. Geophys. Res.* **115** C12050
Schneider A, Tanhua T, Roether W and Steinfeldt R 2014 Changes in ventilation of the Mediterranean Sea during the past 25 years *Ocean Sci.* **10** 1–16
Shabrang L, Menna M, Pizzi C, Lavigne H, Civitarese G and Gačić M 2016 Long-term variability of the southern Adriatic circulation in relation to North Atlantic Oscillation *Ocean Sci.* **12** 233–41
Sunanda N, Kuttippurath J and Chakraborty A 2025 A comparative evaluation of satellite and bio-argo-based net primary productivity algorithms for the north Indian Ocean *Discov. Ocean.* **2** 31
Terzić E, Cardin V, Le Meur J, Dunić N, Vodopivec M and Vilibić I 2025 Unprecedented warming and salinization observed in the deep Adriatic *Limnol. Ocean. Lett.* **10** 888–98
Terzić E and Vilibić I 2026 Twenty-first century thermohaline trends and abrupt shifts in the Ionian Sea *Front. Mar. Sci.* **12** 1718186
Verri G *et al* 2024 Climate projections of the Adriatic Sea: role of river release *Front. Clim.* **6** 1368413
Verri G, Pinardi N, Oddo P, Ciliberti S A and Coppini G 2018 River runoff influences on the Central Mediterranean overturning circulation *Clim. Dyn.* **50** 1675–703
Vilibić I, Mihanović H, Janeković I and Šepić J 2016 Modelling the formation of dense water in the northern Adriatic: sensitivity studies *Ocean Modell.* **101** 17–29
Vilibić I, Pranić P and Denamiel C 2023 North Adriatic Dense Water: lessons learned since the pioneering work of Mira Zore-Armanda 60 years ago *Acta Adriat.* **64** 53–78
Vilibić I, Šepić J and Proust N 2013 Weakening thermohaline circulation in the Adriatic *Sea Clim. Res.* **55** 217–25
Vodopivec M, Zaimi K and Peliz J 2022 The freshwater balance of the Adriatic Sea: a sensitivity study *J. Geophy. Res.* **127** e2022JC018870
von Schuckmann K, Le Traon P-Y, Smith N, Pascual A, Brasseur P, Fennel K and Djavidnia S 2018 Copernicus marine service ocean state report, issue 2 *Journal of Operational Oceanography* **11** s1–142
Wong A P S *et al* 2020 Argo Data 1999–2019: Two million temperature-salinity profiles and subsurface velocity observations from a global array of profiling floats *Front. Mar. Sci.* **7** 700
Wong A P S, Johnson G C and Owens W B 2003 Delayed-mode calibration of autonomous CTD profiling float salinity data by theta-S climatology *J. Atmos. Oceanic Technol.* **20** 308–18
Yari S, Kovačević V, Cardin V, Gačić M and Bryden H L 2012 Direct estimate of water, heat, and salt transport through the Strait of Otranto *J. Geophys. Res. Oceans* **117** 1–14